International Journal of Nanoelectronics and Materials
IJNeaM
ISSN 1985-5761 | E-ISSN 2232-1535


# The effect of treated flue gas desulfurization (FGD) sludge addition on the properties of non-stoichiometric cordierite

Fatin Fatini Othman[a], Banjuraizah Johara[a*], Shing Fhan Khor[b], Nik Akmar Rejab[c] and Suffi Irni Alias[a]

[a]*Faculty of Chemical Engineering Technology, Universiti Malaysia Perlis (UniMAP), 02600 Arau, Perlis, Malaysia*
[b]*Faculty of Electrical Engineering Technology, Universiti Malaysia Perlis (UniMAP), 02600 Arau, Perlis, Malaysia*
[c]*School of Materials and Mineral Resources Engineering, Universiti Sains Malaysia (USM), 14300 Nibong Tebal, Penang, Malaysia*
*∗ Corresponding author. Tel.: +60-019-526-6897; fax: +0-04-979-8178; e-mail: banjuraizah@unimap.edu.my*

Received 18 January 2024, Revised 13 September 2024, Accepted 19 September 2024

**ABSTRACT**

This study examines the incorporation of treated Flue Gas Desulphurization (FGD) by-products from the glass industry in Malaysia into non-stoichiometric cordierite compositions, focusing on its effects on the physical, mechanical, and microstructural properties. New ceramic samples were developed using a blend of kaolin, silica, talc, and treated FGD sludge. The results indicate that increasing the amount of treated FGD sludge leads to desirable properties such as a low thermal coefficient of expansion (2.62 – 3.64 x $10^{-6}$/ ℃), reduced density, and decreased average flexural strength (34.43 – 54.69 MPa), along with an increase in average porosity (17.04 - 31.90 %). Notably, ceramics that were treated with 3 wt% FGD sludge crystallized $\alpha$-cordierite at a lower sintering temperature (1250 ℃), whereas traditional solid-state reaction methods need higher temperatures (>1350 ℃) to make $\alpha$-cordierite. Overall, replacing feldspar with treated FGD sludge in non-stoichiometric cordierite formulations presents a sustainable strategy for recycling industrial waste and reducing the need for natural resources. The resulting materials exhibit characteristics suitable for lightweight construction applications, such as commercial bricks, due to their light weight, adequate flexural strength, and appropriate porosity.

**Keywords:** *ceramic cordierite, FGD sludges, sintering aids.*

## 1. INTRODUCTION

Flue-gas desulfurization (FGD) is a waste incineration process that commonly uses limestone ($CaCO_3$) to eliminate sulfur dioxide ($SO_2$) from power plant flue gas emissions [1]. Nippon Electric Glass Sdn Bhd (NEGM) produces 135 tons of sludge with high sulphur content every month. The sludge is disposed of via landfill at an operating cost of RM400 per ton. Such disposal methods can cause heavy metals to leach into rainwater, contaminating groundwater and rivers [2]. Thus, it is necessary to investigate the potential application of FGD sludge waste to reduce environmental pollution [1]. Numerous researchers have explored the potential of sludge as an alternative material in plaster moulds [3], [4], ceramic production [5], and cement substitutes in soil stabilization [6]. The investigation is crucial for mitigating the environmental issues arising from sludge waste accumulation and converting it into a valuable alternative material in ceramic production.

X-ray fluorescence elemental analysis shows that the FGD obtained from glass manufacturing contains high concentrations of boron and other alkaline oxides in addition to Ca and S. The presence of glass-forming oxides and modifying oxides in the sludge waste powder may act as sintering aids to promote the crystallization of the crystalline ceramic phase.

Cordierite is a valuable crystalline phase in the $MgO$-$Al_2O_3$-$SiO_2$ ternary system. Cordierite can be classified into two major polymorphs, namely α-cordierite and β-cordierite [10],[11], which can be distinguished based on the crystal system and Al-Si ordering [12]. Most natural cordierites form β-cordierite at low temperatures, have an orthorhombic crystal system and a space group symmetry Cccm; while α-cordierite, also known as indialite, forms at high temperatures, has a hexagonal structure with space group symmetry of P6/mcc [13], featuring a disorder of Al-Si distribution [14]. Cordierite has excellent thermal shock resistance, a low thermal expansion coefficient (≤ 4.0 x 106/℃), a low dielectric constant (4.0 – 5.0 at 1 MHz), good chemical durability, excellent refractoriness, and mechanical properties [7],[8],[9], and therefore has many important applications. However, it was difficult to crystallize α-cordierite at a lower temperature since the crystallization temperature is near to its incongruent melting temperature. Therefore, nucleating agents or sintering aids are normally added to enhance the crystallization temperature of the α-cordierite phase.
This study explored a novel approach to replace different amounts of magnesium oxide with treated FGD sludge powder in non-stoichiometric cordierite compositions. Sun

et al. [15] have shown that calcium can substitute magnesium in cordierite systems, facilitating the dissolution of cordierite grains and promoting the formation of anorthite phases. Conversely, Lamara et al. [16] suggested that sintering kaolin-magnesia mixtures without the addition of CaO resulted primarily in the nucleation and growth of monolithic cordierite. This study is innovative as it investigated the use of FGD sludge, which is rich in calcium and also contains B2O3, i.e., a significant glass former and sintering aid, as a potential substitute for MgO to enhance the crystallization of α-cordierite. This substitution could reduce the reliance on MgO and also offer a sustainable solution for managing FGD sludge waste. Despite the promising potential of FGD sludge in modifying ceramic compositions, no studies have tested its use as a sintering aid in cordierite formulations. Therefore, this research addresses this gap and provides new insights into the effects of FGD sludge as a replacement for MgO in cordierite ceramics.

## 2. Materials and Methods

### 2.1. Materials

Raw FGD sludge used was obtained from Nippon Electric Glass Malaysia, NEGM. Silica ($SiO_2$), magnesium oxide (MgO), aluminium oxide ($Al_2O_3$), talc ($3MgO•4SiO_2•H_2O$), and kaolin ($Al_2O_3•2SiO_2•2H_2O$) each with a purity of ≥ 92% were procured from Ipoh Ceramic Sdn Bhd.

### 2.2. Methods

The synthesis of cordierite ceramic using the solid-state reaction method was performed in two steps: (i) the preparation of treated FGD sludge, and (ii) the preparation of non-stoichiometric cordierite composition of $2.8MgO•1.5Al_2O_3•5SiO_2$ incorporating various amounts of treated FGD sludge.

The treated FGD sludge powder was produced through calcination at a temperature of 1100℃ for 3 hours to eliminate any moisture (both physical and crystal water), impurities, organic matter, and unstable gas. The calcine sludge powder was left overnight and then pulverized into fine particles using a Pulverisette 6 machine. The composition of treated FGD sludge in varying percentages (0wt%, 1.5wt%, 3.0wt%, and 4.5wt%) was selected to substitute MgO content in the non-stoichiometric cordierite formulation, as detailed in Table 1. Each composition was accurately weighted and milled using a planetary mill at 300rpmfor 1 hour using tungsten carbide as the grinding medium to ensure a homogenous mixture. The resulting powder mixture was then pressed into a cylindrical die shape with a diameter of 12 mm under a pressure of 11MPa, forming a pellet structure. Next, the samples were sintered at 1250 ℃ for 3 hours at a heating rate of 5℃/min before characterization.

### 2.3. Characterization

X-ray Fluorescence (XRF) was used to detect the chemical composition of the FGD sludges in dried powder. The X-ray diffraction (XRD) patterns of the samples were acquired using Bruker's X-ray Diffraction D8-Discover instrument, operating with Cu-Kα radiation at a wavelength of 1.5418Å, and measurements were conducted in the range of $5° \leq 2\theta \leq 90°$ with a step size of 0.03. Microstructural analysis was performed on the samples at magnifications of 500x and 5000x using a TM3000 Tabletop Scanning Electron Microscope (SEM). Bulk density and apparent porosity were determined using the Archimedes method, with distilled water serving as the
liquid media, as described in reference [18]. The flexural strength was measured using a three-point bend test machine, following the procedure outlined in reference [19]. The coefficient of thermal expansion of the sample was obtained using dilatometry (Model-Linseis DTAPT1600), in the temperature range from 20℃ to 1000 ℃ at a heating rate of 5℃/min.

## 3. Results and Discussion

### 3.1. Chemical properties of treated FGD sludge used in non-stoichiometric cordierite formulation.

The treated FGD sludge powder utilized in this research highly exhibits alkalinity, with a pH of 9.33. This alkalinity primarily arises from the use of limestone (calcium carbonate) in most FGD techniques as an alkali sorbent to capture acidic compounds like sulphur, resulting in the formation of solid alkali particles [2]. Table 2 shows the chemical composition of the raw material used in this research. The primary constituents detected in the treated FGD sludge powder is calcium oxide (CaO), sulphur trioxide ($SO_3$), and aluminium oxide ($Al_2O_3$), constituting 46.9%, 42.2%, and 7.9%, respectively. Additionally, other components including iron (III) oxide ($Fe_2O_3$), chromium (III) oxide ($Cr_2O_3$), and potassium oxide ($K_2O$) are also present.

The addition of CaO in cordierite compositions has been well documented in the literature. Malekzadeh and Rezvani stated that CaO enhances the formation rate and intensity of α-cordierite [20]. N. Ibrahim et al. [21] successfully synthesised α-cordierite with anorthite as a minor phase by adding 5wt% of CaO and sintering at 900℃ using glass methods. Furthermore, CaO has also been employed as an additive to facilitate the nucleation and growth of cordierite. S. Lamara et al. [16] reported that an increase in CaO led to a decrease in the cordierite formation temperature and an increase in the activation energy.

**Table 1.** Sample composition with different weight percentages (wt%) of treated FGD sludge powder used.

| Raw Material | FGD 0 | FGD 1.5 | FGD 3.0 | FGD 4.5 |
|---|---|---|---|---|
| Sludge | 0 | 1.5 | 3.0 | 4.5 |
| Silica | 0.133 | 0.133 | 0.133 | 0.133 |
| Magnesia | 4.50 | 3.00 | 1.50 | 0 |
| Alumina | 4.052 | 4.052 | 4.052 | 4.052 |
| Talc | 29.485 | 29.485 | 29.485 | 29.485 |
| Kaolin | 61.822 | 61.822 | 61.822 | 61.822 |

**Table 2.** Chemical compound of treated FGD sludge used (wt%).

| Materials | CaO | $SO_3$ | $Al_2O_3$ | $Fe_2O_3$ | $Cr_2O_3$ | $K_2O$ | $TiO_2$ | Others |
|---|---|---|---|---|---|---|---|---|
| Treated FGD Sludge | 46.90 | 42.2 | 7.90 | 1.38 | 0.20 | 0.70 | 0.08 | 0.72 |

The presence of silica and alumina in the raw material used in this study provides advantages for the synthesis of high-purity α-cordierite through the solid-state reaction method [22]. However, impurities found in all raw mineral substances such as in mineral talc and kaolin, can hinder the synthesis of high-purity α-cordierite phases [23],[24]. Many researchers have demonstrated that high-purity cordierite can be obtained by incorporating pure silica, alumina, and magnesia in the presence of both talc and kaolin [25],[26].

The XRD patterns of the treated FGD sludge used are presented in Fig. 1. By employing the search match method for phase identification, the treated NEGM's FGD sludge exhibits the presence of anhydrite phase, CaSO4 (ICSD 98-000-5306) with the most intense peak at 2θ = 25.42° [002], 2θ = 31.18° [021], and 2θ = 38.76° [022]. On the other hand, gypsum, $CaSO_4 \bullet 2H_2O$ (ICSD 98-001-1992) has a density of 1.99 g/cm$^3$ with the most intense peaks at 2θ = 28.24°, which corresponds to the plane [22-1] only. The XRD and XRF results for the sludge are consistent with each other, reflecting that the predominant compounds in the sludge were CaO and $SO_3$.

The crystal system of the cordierite phase in sample FGD 0 and sample FGD 1.5 is orthorhombic with space group Ccm, whereas sample FGD 3.0 and sample FGD 4.5 exhibit a hexagonal crystal system with space group of P6/mcc. Furthermore, only β-cordierite has an additional peak at 2θ = 15°, which corresponds to the plane (111), while α-cordierite lacks this peak. Although both α-cordierite and β-cordierite show an almost similar pattern, there is a distinct intensity peak located at 2θ = 21.71°, that belongs to the plane (112). α-cordierite records a lower intensity peak compared to β-cordierite, with a difference of 18.4%. The precise quantification of both α-cordierite and β-cordierite in each sample is challenging due to the severe overlap in their peak positions.

### 3.2. Effect of sludge addition on the phase transformation and crystallization of cordierite ceramic.

Fig. 2 demonstrates XRD patterns for four non-stoichiometric cordierite samples prepared by adding different amounts of treated FGD sludge powder. It is evident that each sample distinctly exhibits the presence of α-cordierite ($Al_4Mg_2O_{18}Si_5$) or β-cordierite ($Al_4Fe_{0.86}Mg1.14O_{18}Si_5$) with the most intense peak at 2θ = 10.48°. Additionally, minor phases such as forsterite, sillimanite, and anorthite are also detected in the sintered sample. Notably, the highest peak of forsterite ($Mg_2SiO_4$) diffracted at 2θ = 20.48° crystallized in sample FGD 0 and FGD 1.5 only. Sillimanite ($Al_2O_5Si$) phase, with the most intense peak at 2θ = 60.13°, is observed in samples FGD 0 and FGD 1.5, while anorthite ($CaAl_2Si_2O_8$), with the most intense peak at 2θ = 21.99° begins to crystallize at samples FGD 3.0 and FGD 4.5. A detailed phase analysis of the sintered samples is tabulated in Table 3, and the quantitative analysis of each sample sintered at 1250°C obtained by refining XRD data can be seen in Table 4.

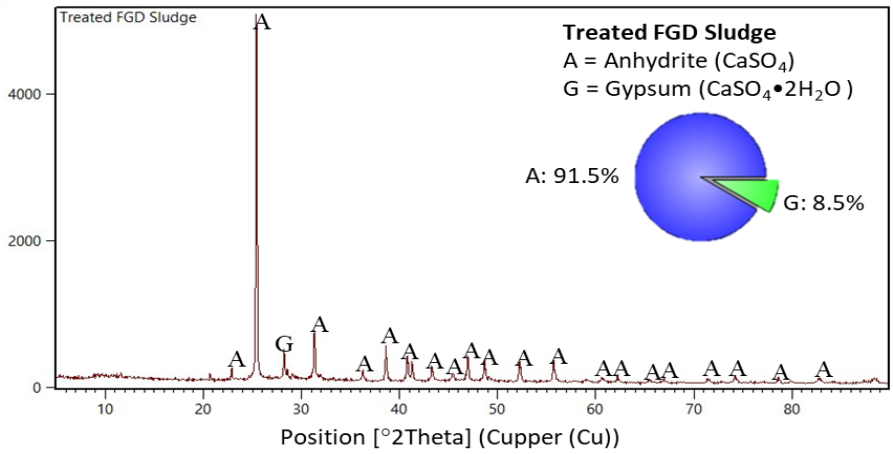


**Figure 1.** The X-ray diffraction patterns of treated FGD sludge. A = anhydrite, G = gypsum

The sample FGD 0 is a pure non-stoichiometric cordierite composition that exhibits a limited ability to crystallize α-cordierite phases through solid-state methods, indicating that the composition requires a higher sintering temperature. The formation of α-cordierite phase gradually increased with increasing treated FGD sludge powder in the mixture but began to decrease in sample FGD 4.5 because the anorthite phase started to grow with the increase in CaO molar ratio in the sample composition. On the other hand, the formation of forsterite decreases with a decreasing amount of MgO. In conclusion, β-cordierite is present in FGD 0 and FGD 1.5 while α-cordierite is exclusively found in FGD 3.0 and FGD 4.5.

For better observation, the XRD pattern for FGD 3.0 was focused on 2θ ranging between 9° and 80°, as shown in Fig. 3. These peaks could not be observed as clearly in Fig. 2, as the intensity of the cordierite phase located at 2θ = 10.45°, corresponding to the plane (110) for FGD 3.0 is abnormally higher than the other samples. Minor phases such as forsterite and sillimanite tend to crystallize at low sintering temperatures in comparison to FGD 3.0 and FGD 4.5. This behavior can be attributed to the excess MgO content in the composition of samples FGD 0 and FGD 1.5. The presence of forsterite and sillimanite indicates that the complete diffusion of atoms does not occur since Al, Si, and Mg atoms form two different compounds. The absence of a glassy phase or fluxing compound during the sintering process impedes the diffusion of atoms and the formation of stable compounds. The most pronounced peak of forsterite is detectable at 2θ = 20.48°, corresponding to the plane (010), while the strongest peak of the sillimanite phase diffracted at 2θ = 60.13°, which belongs to the plane (033). When the concentration of treated FGD sludge powder exceeds 4.0 wt.% in the composition, the anorthite phase begins to crystallize. The strongest anorthite peak is observed at 2θ = 21.99°, corresponding to the plane (200). In this case, the formation of anorthite depends on the balance between $Al_2O_3$ and CaO in the $CaO\text{-}Al_2O_3\text{-}SiO_2$ field [27]. In the presence of CaO, minor phases such as fosterite and sillimanite phase tend to recrystallize into more stable phases such as cordierite.

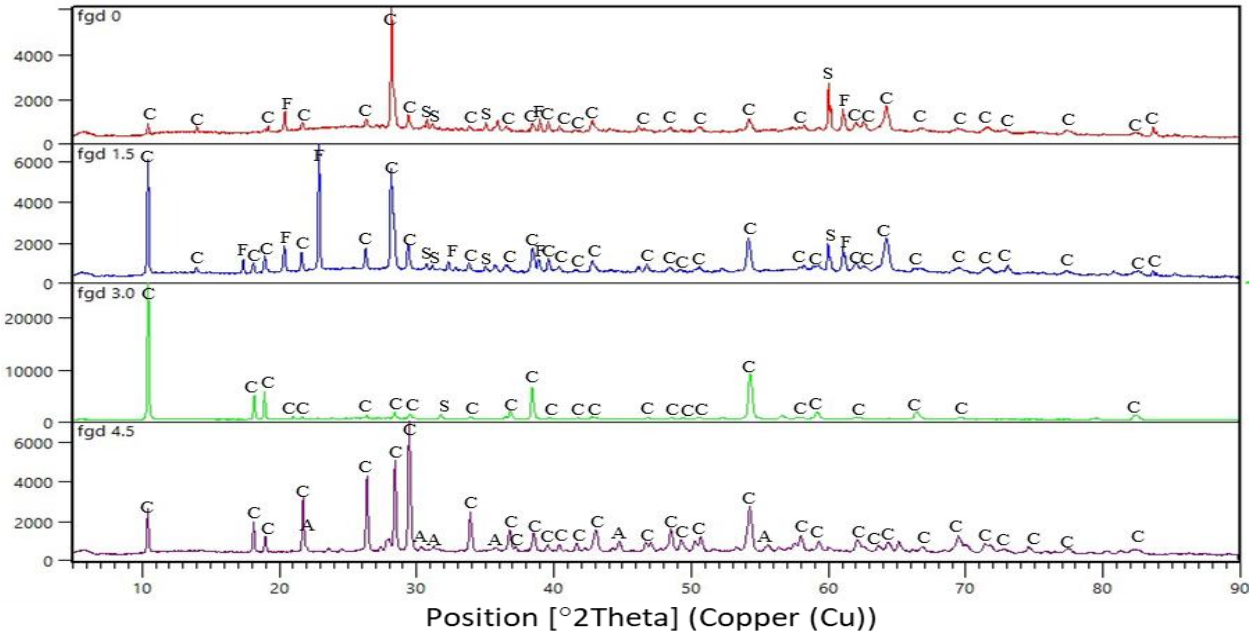


**Figure 2.** The X-ray diffraction patterns of the sintered samples at 1250 ℃ with different sludge content.
C = cordierite, F = forsterite, S = sillimanite, A = anorthite.

**Table 3.** The phase analysis of sintered samples with different amounts of treated FGD sludge.
H = Hexagonal, O = Orthohombic, A = Anorthic.

| Samples | Porosity (%) | Density (g/m$^3$) | Flexural strength (MPa) | Volume shrinkage (%) | Coefficient of thermal expansion (℃$^{-1}$) |
|---|---|---|---|---|---|
| FGD 0 | 20.31 | 2.48 | 54.69 | 31.00 | 1.82 x 10$^{-6}$ |
| FGD 1.5 | 17.04 | 2.44 | 45.75 | 25.07 | 0.98 x 10$^{-6}$ |
| FGD 3.0 | 27.05 | 2.36 | 41.12 | 17.61 | 2.24 x 10$^{-6}$ |
| FGD 4.5 | 31.90 | 2.67 | 34.43 | 16.54 | -1.16 x 10$^{-6}$ |

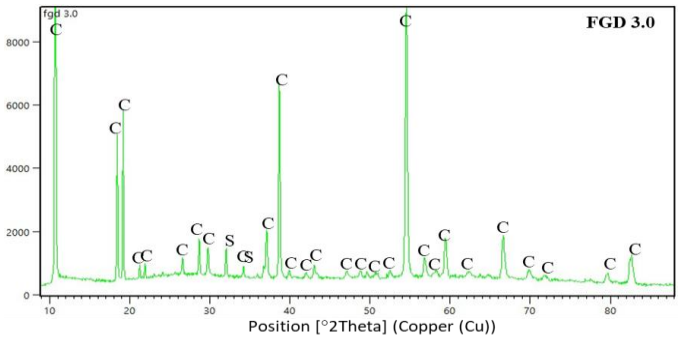


**Figure 3.** Full scale of XRD pattern for sample FGD 3.0.

Increasing the amount of treated sludge substitution resulted in a more intense peak of the cordierite phase at 2θ = 10.45°, which belongs to the plane (110), but it deteriorates as the concentration of FGD sludge powder substitution reaches 4.5 wt.%. The difference in the intensity peak of each sample diffracted at 2θ = 10.45° and their respective percentages (%) are presented in Fig. 4. According to Fig. 4, the increase was 88.57% for FGD 1.5, 97.59% for FGD 3.0, and 70.91% for FGD 4.5. Since the testing parameters remain constant, the higher intensity peak observed in the plane (110) might be due to the preferred orientation, crystal growth direction pattern, or the presence of impurities element substitution on that specific plane [28].

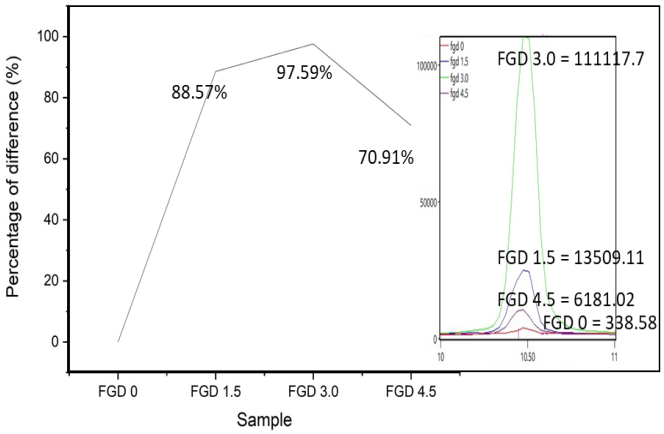


**Figure 4.** The intensity peak of each sample diffracted at 2θ = 10.45° [110] and their percentage of difference (%).

Fig. 5 shows the microstructure of all sintered cordierite samples with and without FGD sludge powder addition. As the amount of treated sludge increases, the presence of pores inside the sample increases. However, a large number of irregular particles accumulate in the pores in the internal structure of the sample sintered at 1250°C, indicating that the sintered sample is not fully densified.

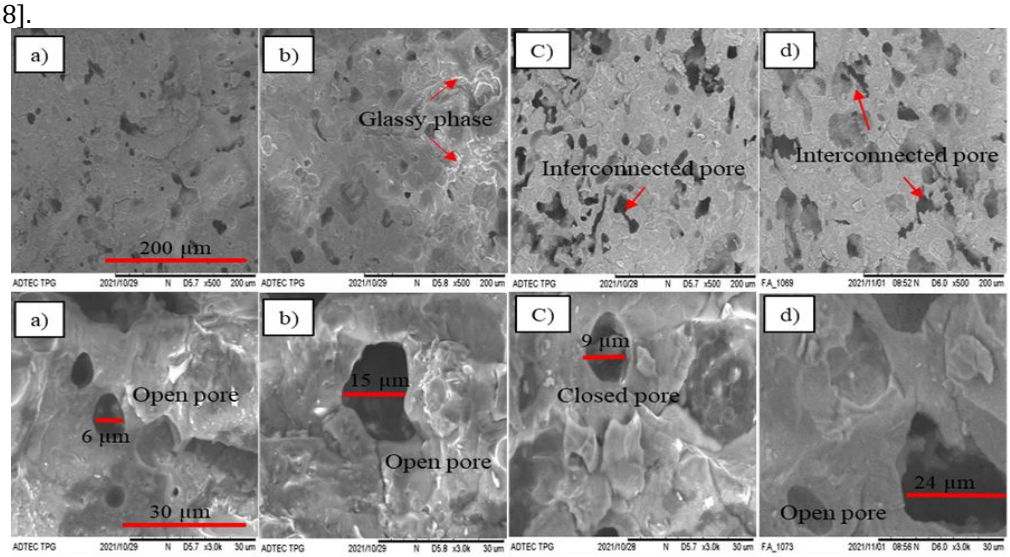


**Figure 5.** The scanning electron microscopy (SEM) images of the samples sintered at 1250°C with different sludge contents at a magnification of 500x (left) and 5000x (right) (a) FGD 0, (b) FGD 1.5, (c) FGD 3.0, and (d) FGD 4.5.

As demonstrated in Table 2, the XRF analysis of the treated FGD sludge powder reveals a sulfur trioxide ($SO_3$) content of 42.2 %. Therefore, increasing the amount of treated FGD sludge added to the composition resulted in a higher pore content in the samples. Sample FGD 3.0 and FGD 4.5 exhibited interconnected pores due to the addition of a large amount of treated sludge. All samples with treated FGD sludge addition exhibit the formation of super-micropores, as the pore sizes of sample FGD 1.5, FGD 3.0, and FGD 4.5 fall within the range of 10 μm to 100 μm, while the pores in FGD 0 can be classified as inter-micropore since their sizes range from 1 μm to 10 μm [29].

XRF results showed that despite the thermal treatment of FGD sludge powder at a calcination temperature of 1100°C, sulfur dioxide ($SO_2$) gas could not be completely decomposed. According to Sievert et al. [30], anhydrite remains thermodynamically stable up to 1180 ℃, and as suggested by Z. Wang et al. [31], the decomposition of $CaSO_4$ occurs at around 1150 ℃. Thus, the decomposition of $SO_2$ takes place during the sintering of the sample, leading to the formation of pores in the internal structure of samples with the addition of treated FGD sludge. Moreover, an increased amount of treated FGD sludge in the samples also results in the creation of larger pores. The gradual decomposition of gas to form pores during sintering is a beneficial method for preparing porous ceramics. High-strength porous ceramic materials are advantageous for building structural applications because the thermal conductivity of the material can be effectively reduced.

As depicted in Fig. 5b, the microstructure of sample FGD 1.5 exhibits a significant amount of glass phases, primarily due to its higher porosity content compared with FGD 3.0 and FGD 4.5, resulting in unobstructed grain boundaries [32]. Notably, the increase in the FGD sludge powder addition leads to a substantial increase in the quantity of liquid phases. These liquid phases play a crucial role in the sintering process of the α-cordierite phase at 1250℃ by wetting the raw particles and accelerating ion transport [33]. A discernible amount of liquid phase is visible in Fig.3d. The interaction between calcium (Ca) and silicon dioxide ($SiO_2$) in the sludge successfully forms a silicon-rich molten glass phase at a lower sintering temperature [34], especially at 1250℃.

### 3.3. Effect of sludge addition on the physical and thermal characteristics of cordierite ceramic.

Table 4 presents the properties of the sintered samples prepared with varying weight percentages of FGD-treated sludge powder. As shown in Table 4, the porosity values of the samples at different quantities of sludge are in agreement with the SEM morphology displayed in Fig. 3. The porosity of the samples decreases with the addition of 1.5 wt% of sludge, but it continues to increase with the addition of 3.0 wt% and 4.5 wt%.

Furthermore, the density of the samples decreases with the increasing quantity of treated FGD sludge powder and experiences a sharp increase in the case of sample FGD 4.5. This phenomenon can be attributed to the presence of minor phases in the cordierite ceramic bodies, each with its distinct density. Fosterite and sillimanite have densities of 3.22 g/cm$^3$ and 3.17 g/cm$^3$, respectively. Meanwhile, samples FGD 0 and FGD 1.5 exhibit moderately lower densities compared to the theoretical density of the phases, owing to the formation of pores leading to a reduction in sample density. Theoretically, pure α-cordierite has a density of 2.52 g/cm$^3$, while the sample with the most crystallized α-cordierite, i.e., sample FGD 3.0 has the lowest density of 2.36 g/cm$^3$. Sample FGD 3.0 displays a slightly lower density value than the theoretical value of cordierite's density due to the presence of pores in the sample. The formation of anorthite phase, which aligns with the theoretical density value of 2.76 g/cm$^3$, occurred in sample FGD 4.5. This explains the increase in the density value of the sample, even though it had a higher pore content. Therefore, the density of the sample is predominantly influenced by the theoretical density of each phase and the presence of pores in the sintered samples.

As stated in Table 4, the flexural strength of the samples decreases with the increasing amount of treated FGD sludge powder addition. This decline is attributed to the decomposition of SO3 during sintering, which leads to an increase in the porosity of cordierite as the treated FGD sludge rises. Lian et al. [35] emphasized that the strength of porous materials is significantly affected by the porosity within their internal structure. The presence of a substantial volume of air voids in porous materials can weaken the bonding of the internal component [36], thus diminishing the materials' ability to withstand pressure. The theoretical flexural strength of cordierite stands at 66 MPa, However, the flexural strength of all the examined samples displays a decreasing trend due to the presence of minor phase and porous internal structure.

**Table 4.** Properties of the sintered samples at 1250 ℃ with different treated sludge contents.

| Samples | Porosity (%) | Density (g/m$^3$) | Flexural strength (MPa) | Volume shrinkage (%) | Coefficient of thermal expansion (℃$^{-1}$) |
|---|---|---|---|---|---|
| FGD 0 | 20.31 | 2.48 | 54.69 | 31.00 | 1.82 x 10$^{-6}$ |
| FGD 1.5 | 17.04 | 2.44 | 45.75 | 25.07 | 0.98 x 10$^{-6}$ |
| FGD 3.0 | 27.05 | 2.36 | 41.12 | 17.61 | 2.24 x 10$^{-6}$ |
| FGD 4.5 | 31.90 | 2.67 | 34.43 | 16.54 | -1.16 x 10$^{-6}$ |

In addition, as seen in Table 4, all the samples exhibit a diminishing trend in shrinkage and a denser internal structure. Surprisingly, despite having a lower pore concentration, sample FGD 1.5 displays lower flexural strength compared to FGD 0. This is due to the slower rate of shrinkage, rendering sample FGD 1.5 unable to form a dense body capable of withstanding a load. The SEM images also demonstrate that the pore size of FGD 1.5 is significantly larger than that of FGD 0, which accounts for the reduction in flexural strength. Nonetheless, the relatively low flexural strength of cordierite ceramic does not impede its use in common applications such as heating elements, resistors, band heaters, ovens, furnaces, and fuses [10]. It is also suitable to be used as a brick because the minimum standard requirement for a commercial brick is only 5 MPa [37].

Fig. 6 illustrates the thermal expansion of sintered cylindrical pellets with varying compositions of treated FGD sludge. A dilatometer test was conducted on all sintered samples, spanning from room temperature to 1000 ℃, with a heating rate of 5 ℃/min to determine the coefficient of thermal expansion (CTE). As highlighted by R. Wool et al. [31], CTE results provide insights into the average atomic spacing changes with increasing temperature, offering a perspective at the atomic level. Typically, materials with weaker bonds tend to exhibit higher CTE values, reflecting changes in bond length as temperature rises. Furthermore, Ardebili et al. [38] noted that the thermal expansion rate varies with material types, as different materials expand differently at the same heating rate due to the attachment of different arrangements of elements in the structure as a function of temperature.

The dilatometric curve provides valuable insights into the sintering reaction of the materials, revealing a three-phase process: shrinkage from room temperature to 200 ℃, expansion from 200 ℃ to 780 ℃, and shrinkage from 780 ℃ to 1000 ℃. Despite the samples being stored under sealed conditions, the presence of clay minerals such as kaolin, known for its substantial specific surface areas, allows for water absorption by the samples [39]. In addition, the formation of slaked lime (calcium hydroxide, Ca(OH)2) takes place due to CaO's affinity for water absorption at room temperature [40]. The chemical reaction for this process is shown in Equation 1. Notable, sample FGD 3.0 exhibits a lower rate of shrinkage, with a CTE value of -3.72 x $10^{-6}$/℃ compared to other samples, reflecting its modest volume fluctuations and lower water absorption capabilities.

$$CaO + H_2O \rightarrow Ca(OH)_2 \quad (1)$$

The second phase of the sintering reaction commences at 200 ℃, with all samples experiencing thermal expansion. During this stage, grain development takes place, which affects densification. C. Maniere et al. (2018) reported that grain expansion slows down the sample densification as grain size directly affects the diffusional path of segregation. Notably, two distinct CTE values are detected within the temperature range 200 ℃ to 400 ℃ on samples FGD 0 and FGD 1.5 displaying similar rates of expansion (CTE values of 3.64 x 10-6/℃ and 3.53 x 10-6/℃, respectively). In contrast, samples FGD 3.0 and FGD 4.5 exhibit lower CTE values, indicating the presence of a high amount of α-cordierite crystalline phase in these samples. Both samples recorded a CTE value of 2.62 x 10-6/℃ and 2.70 x 10-6/℃, respectively. The theoretical CTE value of α-cordierite is notably lower (approximately 1.5 x 10-6/℃ to 4.0 x 10-6/℃) than other phases present in the samples, which is due to the rigid tetrahedral framework and anisotropic expansion of the octahedral framework of the α-cordierite structure, making it capable of withstanding high temperature with minimal volume change [42][43].

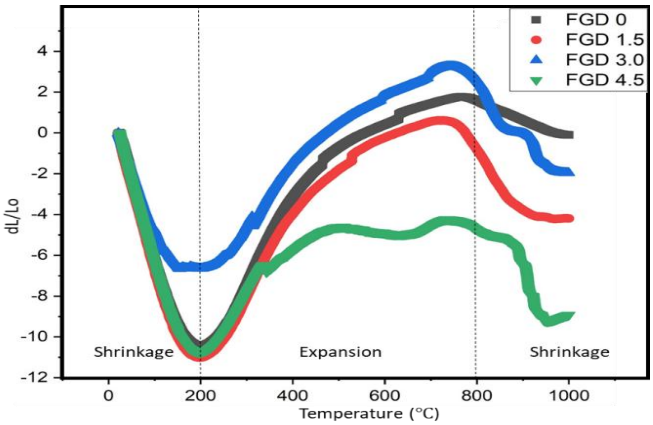


**Figure 6.** Dilatometric curve of sintered cylindrical pellets with various treated FDG sludge compositions.

When compared to the early stages of expansion, the second rate of expansion of all samples shows a decrement even at high sintering temperatures. According to R. Khattab et al. [44], factors contributing to this decrease in thermal expansion include the development of microcracks due to the difference in thermal expansion between the glassy phase and the matrix, lattice thermal anisotropy, and the presence of pores in the sample structure. At this stage, grain growths in all samples begin to slow, indicating the activation of glassy phase formation in the sample. The presence of numerous large pores in the sample with treated FGD sludge explains this occurrence. Importantly, this grain growth takes place within the pore and does not affect the overall volume changes of the sample.

The third and final phase extends up to 780 ℃ for samples FGD 0, FGD 1.5, and FGD 3.0 while FGD 4.5 starts at 890 ℃, at which all samples commence shrinking. The softening temperature for each sample can be explained during this phase. Here, the fluxing element and glass former, like CaO and B2O3, respectively, in the treated FGD sludge begin to melt and produce a glassy phase. This glassy phase diffuses between the atoms, reducing the gaps between grains and facilitating the crystallization of the most equilibrium compound. Notably, sample FGD 4.5 achieves a higher softening temperature due to the presence of larger pores and requires a higher temperature to produce a sufficient

glassy phase to diffuse between the grains. This explanation aligns with M.J. Pomeroy [45], where glass softening temperature (TD) coincides with rapid contraction of sample length. Table 5 shows the changes in thermal expansion coefficients of samples throughout the stages of dimensional changes as a function of treated FGD sludge substitution in non-stoichiometric cordierite composition.

**Table 5.** Coefficient of thermal expansion of sample as a function of treated sludge addition at each stage of dimensional changes.

| Stages | | CTE value (x $10^{-6}$/°$C^{-1}$) | | | |
|---|---|---|---|---|---|
| | | Shrinkage | Expansion 1 | Expansion 2 | Shrinkage |
| Temperature (°C) | | 30 - 200 | 200 – 400 | 400 - 780 | 780 - 1000 |
| Sample | FGD 0 | -5.92 | 3.64 | 1.28 | -0.83 |
| | FGD 1.5 | -6.11 | 3.53 | 1.37 | -1.80 |
| | FGD 3.0 | -3.72 | 2.62 | 1.31 | -2.12 |
| | FGD 4.4 | -6.09 | 2.70 | 0.25 | -2.81 |

G. H. Chen [46] reported that the addition of raw CaO to cordierite composition resulted in the formation of α-cordierite with a higher CTE value (4.00 x 10-6/°C - 4.25 x 10-6/°C) compared to the reference sample without CaO. Conversely, the incorporation of CaO derived from treated FGD sludge facilitated the crystallization of the α-cordierite phase, yielding a remarkably low thermal expansion (CTE value; 2.62 with 3.0 wt% of treated FGD sludge addition), well below the reported CTE value of 4.0 x 10-6/°C and lower. Therefore, the addition of treated FGD sludge offers substantial benefits to produce α-cordierite ceramics, particularly high-refractory porous bricks.

## 4. Conclusion.

In conclusion, samples sintered at 1250 °C for 3 hours have revealed severely noteworthy findings. These samples exhibit high porosity, low density, moderate flexural strength, and a notable low coefficient of thermal expansion. Rietveld analysis confirms that cordierite is the primary crystalline phase (β-cordierite: FGD 0 and FGD 1.5, α-cordierite: FGD 3.0 and FGD 4.5), with the manifestation of minor phases such as fosterite and sillimanite in sample FGD 0 and FGD 1.5 and anorthite in sample FGD 3.0 and FGD 4.5. Of all samples sample FGD 3.0 demonstrated the most favorable performance with an impressive composition of 89.6wt% of α-cordierite and 10.4 wt% of sillimanite alongside an exceptionally CTE value of 2.24 x 10-6/°C. The empirical results underscore the potential for the cost-effective crystallization of α-cordierite through the solid-state method, even at a relatively low sintering temperature of 125 °C, by utilizing desulfurized sludge as CaO precursor that also contains B2O3 that functions as nucleating agent and sintering aids. Notably from an environmental perspective, the utilization of FGD sludge in the synthesis of cordierite offers a significant advantage by facilitating industrial waste before it reaches landfills and reduces the demand for natural resources. This approach exemplifies a sustainable and eco-friendly solution with far-reaching implications for materials science and environmental conservation.

## ACKNOWLEDGEMENTS

The authors acknowledge the financial support provided by the Ministry of Higher Education through the Fundamental Research Grant Scheme (FRGS) under a grant number of FRGS/1/2019/STG07/UNIMAP/02/4. The authors also would like to thank Nippon Electric Glass Sdn. Bhd. for providing the FGD sludge.

## REFERENCES

[1] K. Tabit, M. Waqif, and L. Saâdi, "Anorthite-cordierite based binary ceramics from coal fly ash and steel slag for thermal and dielectric applications," Mater. Chem. Phys., vol. 254, 2020.

[2] I. Suárez-Ruiz and C. R. Ward, "Coal Combustion," Appl. Coal Petrol., pp. 85–117, 2008.

[3] C. Chandara, K. A. M. Azizli, Z. A. Ahmad, and E. Sakai, "Use of waste gypsum to replace natural gypsum as set retarders in portland cement," Waste Manag., vol. 29, no. 5, pp. 1675–1679, 2009.

[4] B. Guan, H. Fu, J. Yu, G. Jiang, B. Kong, and Z. Wu, "Direct transformation of calcium sulfite to α-calcium sulfate hemihydrate in a concentrated Ca-Mg-Mn chloride solution under atmospheric pressure," Fuel, vol. 90, no. 1, pp. 36–41, 2011.

[5] S. K. Amin, E. M. Abdel Hamid, S. A. El-Sherbiny, H. A. Sibak, and M. F. Abadir, "The use of sewage sludge in the production of ceramic floor tiles," HBRC J., vol. 14, no. 3, pp. 309–315, 2018.

[6] X. C. Qiao, C. S. Poon, and C. Cheeseman, "Use of flue gas desulphurisation (FGD) waste and rejected fly ash in waste stabilization/solidification systems," Waste Manag., vol. 26, no. 2, pp. 141–149, 2006.

[7] J. R. González-Velasco, R. Ferret, R. López-Fonseca, and M. A. Gutiérrez-Ortiz, "Influence of particle size distribution of precursor oxides on the synthesis of cordierite by solid-state reaction," Powder Technol., vol. 153, no. 1, pp. 34–42, 2005.

[8] A. Chowdhury, S. Maitra, S. Das, A. Sen, G. K. Samanta, and P. Datta, "Synthesis, properties and applications of cordierite ceramics, Part 1," InterCeram Int. Ceram. Rev., vol. 56, no. 1, pp. 18–22, 2007.

[9] P. Amista, M. Cesari, A. Montenero, G. Gnappi, and L. Lan, "Crystallization behaviour in the system MgO

Al2O3 SiO2," J. Non. Cryst. Solids, vol. 192–193, pp. 529–533, 1995.
[10] A. Chowdhury, S. Maitra, H. S. Das, A. Sen, G. K. Samanta, and P. Datta, "Synthesis, properties and applications of cordierite ceramics, part 2," InterCeram Int. Ceram. Rev., vol. 56, no. 2, pp. 98–102, 2007.
[11] H. F. Levin, E.M.; McMurdie, "Phase diagrams for ceramists, 1975 supplement," Am. Ceram. Soc., p. 515, 1975.
[12] U. Haefeker, R. Kaindl, P. Tropper, H. Krüger, V. Kahlenberg, and M. Orlova, "Structural investigations of the two polymorphs of synthetic Fe-cordierite and Raman spectroscopy of hexagonal Fe-cordierite," Mineral. Petrol., vol. 108, no. 4, pp. 469–478, 2014.
[13] A. Miyashiro, "Cordierite-indialite relations," Am. J. Sci., vol. 255, no. 1, pp. 43–62, 1957.
[14] G. V Gibbs, "The polymorphism of cordierite. I. The crystal structure of low cordierite," Am Miner., vol. 51, no. 7, pp. 1068–1087, 1966.
[15] Y. Sun et al., "Preparation and strengthening mechanism of prestressed ceramic tile components," Int. J. Appl. Ceram. Technol., 2021.
[16] S. Lamara, D. Redaoui, F. Sahnoune, M. Heraiz, and N. Saheb, "Formation of anorthite containing cordierite materials through reaction sintering kaolin, mgo and cao precursors," Sci. Sinter., vol. 52, no. 2, pp. 135–147, 2020.
[17] M. A. Camerucci, G. Urretavizcaya, and A. L. Cavalieri, "Sintering of cordierite based materials," Ceram. Int., vol. 29, no. 2, pp. 159–168, 2003.
[18] A. Standard, "Refractories and Refractory Materials - Physical test methods, Method 5: The determination of density, porosity and water absorption: 1774.5," 1989.
[19] S. Safiee, H. Md Akil, A. A. M. Mazuki, Z. A. M. Ishak, and A. A. Bakar, "Properties of pultruded jute fiber reinforced unsaturated polyester composites," Adv. Compos. Mater., vol. 20, no. 3, pp. 231–244, 2011.
[20] H. Malekzadeh and M. Rezvani, "Effect of CaO additive on sintering and crystallization behavior of cordierite glass-ceramic prepared by sol-gel method," J. Sol-Gel Sci. Technol., vol. 66, no. 2, pp. 199–205, 2013.
[21] N. Ibrahim, H. Mohamad, Z. A. Ahmad, and J. Banjuraizah, "Effect of cao from different sources on the nanostructured cordierite," Adv. Mater. Res., vol. 364, pp. 368–371, 2012.
[22] H. Li, C. Li, and L. Wu, "Porous cordierite ceramics prepared by foam-gelcasting technique: Phase evolution and properties," J. Alloys Compd., vol. 791, pp. 690–699, 2019.
[23] M. L. Sandoval, M. A. Camerucci, and A. G. T. Martinez, "High-temperature mechanical behavior of cordierite-based porous ceramics prepared by modified cassava starch thermogelation," J. Mater. Sci., vol. 47, no. 23, pp. 8013–8021, 2012.
[24] Y. Ma, J. Li, X. Wang, L. Liu, and C. Wang, "Highly permeable macroporous cordierite ceramics with controlled microstructure produced by particle-stabilized emulsions with a reactive thermal treatment," J. Eur. Ceram. Soc., vol. 37, no. 9, pp. 3203–3211, 2017.
[25] J. Banjuraizah, H. Mohamad, and Z. A. Ahmad, "Crystal structure of single phase and low sintering temperature of α-cordierite synthesized from talc and kaolin," J. Alloys Compd., vol. 482, no. 1–2, pp. 429–436, 2009.
[26] E. P. de Almeida, I. P. de Brito, H. C. Ferreira, H. de L. Lira, L. N. de Lima Santana, and G. de Araújo Neves, "Cordierite obtained from compositions containing kaolin waste, talc and magnesium oxide," Ceram. Int., vol. 44, no. 2, pp. 1719–1725, 2018.
[27] J. C. Hower et al., "Generation and nature of coal fly ash and bottom ash," in Coal Combustion Products (CCPs): Characteristics, Utilization and Beneficiation, 2017, pp. 21–65.
[28] M. Inoue and I. Hirasawa, "The relationship between crystal morphology and XRD peak intensity on CaSO4·2H2O," J. Cryst. Growth, vol. 380, pp. 169–175, 2013.
[29] T. J. Mays, "A new classification of pore sizes," Stud. Surf. Sci. Catal., vol. 160, pp. 57–62, 2007.
[30] T. Sievert, A. Wolter, and N. B. Singh, "Hydration of anhydrite of gypsum (CaSO4.II) in a ball mill," Cem. Concr. Res., vol. 35, no. 4, pp. 623–630, 2005.
[31] Z. Wang et al., "Thermochemical behavior of three sulfates (CaSO4, K2SO4 and Na2SO4) blended with cement raw materials (CaO-SiO2-Al2O3-Fe2O3) at high temperature," J. Anal. Appl. Pyrolysis, vol. 142, 2019.
[32] C. Z. Zhe Chen, Zhongkai Xu, Fengdan Cui, Jian Zhang, Xiaohong Sun, Yunpeng Shang, Rusiong Gue, Nan Liu, Shu Cai, "Direct ink writing of cordierite ceramics with low thermal expansion coefficient," J. Eur. Ceram. Soc., 2021.
[33] L. Wang et al., "Phase-engineering strategy of ZrO2 for enhancing the mechanical properties of porous cordierite ceramics," Mater. Today Commun., vol. 30, 2022.
[34] L. Yuan, B. Ma, Q. Zhu, Z. Wang, G. Li, and J. Yu, "Preparation and properties of MgAl2O4 based ceramics reinforced with rod-like microcrystallines by co-doping Sm2O3 and La2O3," Ceram. Int., vol. 43, no. 18, pp. 16258–16263, 2017.
[35] C. Lian, Y. Zhuge, and S. Beecham, "The relationship between porosity and strength for porous concrete," Constr. Build. Mater., vol. 25, no. 11, pp. 4294–4298, 2011.
[36] L. Li and M. Aubertin, "A general relationship between porosity and uniaxial strength of engineering materials," Can. J. Civ. Eng., vol. 30, no. 4, pp. 644–658, 2003.
[37] B. De Rosa and G. Cultrone, "Assessment of two clayey materials from northwest Sardinia (Alghero district, Italy) with a view to their extraction and use in traditional brick production," Appl. Clay Sci., vol. 88–89, pp. 100–110, 2014.
[38] H. Ardebili, J. Zhang, and M. G. Pecht, "Characterization of encapsulant properties," Encapsulation Technol. Electron. Appl., pp. 221–258, 2018.
[39] A. F. Gualtieri, "Thermal behavior of the raw materials forming porcelain stoneware mixtures by combined optical and in situ X-ray dilatometry," J. Am. Ceram. Soc., vol. 90, no. 4, pp. 1222–1231, 2007.
[40] A. S. Wagh, "Chapter 13 - Calcium Phosphate Cements," Chem. Bond. Phosphate Ceram., pp. 143–155, 2004.
[41] C. Manière, S. Chan, G. Lee, J. McKittrick, and E. A. Olevsky, "Sintering dilatometry based grain growth assessment," Results Phys., vol. 10, pp. 91–93, 2018.
[42] S. S. V. S. S. Vepa and A. M. Umarji, "Effect of Substitution of Ca on Thermal Expansion of Cordierite (Mg2Al4Si5O18)," J. Am. Ceram. Soc., vol. 76, no. 7, pp. 1873–1876, 1993.
[43] B. P. Saha, R. Johnson, I. Ganesh, G. V. N. Rao, S. Bhattacharjee, and Y. R. Mahajan, "Thermal anisotropy in sintered cordierite monoliths," Mater. Chem. Phys., vol. 67, no. 1–3, pp. 140–145, 2001.
[44] R. M. Khattab et al., "Sintering, physicomechanical, thermal expansion and microstructure properties of cordierite ceramics based on utilizing silica fume waste," Mater. Chem. Phys., vol. 270, 2021.
[45] M. J. Pomeroy, "Thermal analysis techniques for technical ceramics and glasses," Encycl. Mater. Tech. Ceram. Glas., vol. 1–3, pp. 676–688, 2021.

[46] G. H. Chen, "Sintering, crystallization, and properties of CaO doped cordierite-based glass-ceramics," J. Alloys Compd., vol. 455, no. 1–2, pp. 298–302, 2008.